

RESEARCH ARTICLE



Mesenchymal stromal cell-derived small extracellular vesicles restore lung architecture and improve exercise capacity in a model of neonatal hyperoxia-induced lung injury

Gareth R. Willis^{a,b}, Angeles Fernandez-Gonzalez^{a,b}, Monica Reis^{a,b}, Vincent Yeung^{a,b}, Xianlan Liu^a, Maria Ericsson^c, Nick A. Andrews^d, S. Alex Mitsialis^{a,b} and Stella Kourembanas^{a,b}

^aDivision of Newborn Medicine & Department of Pediatrics, Boston Children's Hospital, Boston, MA, USA; ^bDepartment of Pediatrics, Harvard Medical School, Boston, MA, USA; ^cDepartment of Cell Biology, Harvard Medical School, Boston, MA, USA; ^dF.M. Kirby Center for Neurobiology, Harvard Medical School, Boston Children's Hospital, Boston, MA, USA

ABSTRACT

Early administration of mesenchymal stromal cell (MSC)-derived small extracellular vesicles (MEx) has shown considerable promise in experimental models of bronchopulmonary dysplasia (BPD). However, the ability of MEx to reverse the long-term pulmonary complications associated with established BPD remains unknown. In this study, MEx were isolated from media conditioned by human Wharton's Jelly-derived MSC cultures. Newborn mice (FVB strain) were exposed to hyperoxia (HYRX (75% O₂)) before returning to room air at postnatal day 14 (PN14). Following prolonged HYRX-exposure, animals received a single MEx dose at PN18 or serial MEx treatments at PN18-39 ("late" intervention). This group was compared to animals that received an early single MEx dose at PN4 ("early" intervention). Animals were harvested at PN28 or 60 for assessment of pulmonary parameters. We found that early and late MEx interventions effectively ameliorated core features of HYRX-induced neonatal lung injury, improving alveolar simplification, pulmonary fibrosis, vascular remodelling and blood vessel loss. Exercise capacity testing and assessment of pulmonary hypertension (PH) showed functional improvements following both early and late MEx interventions. In conclusion, delivery of MEx following prolonged HYRX-exposure improves core features of experimental BPD, restoring lung architecture, decreasing pulmonary fibrosis and vascular muscularization, ameliorating PH and improving exercise capacity. Taken together, delivery of MEx may not only be effective in the immediate neonatal period to prevent the development of BPD but may provide beneficial effects for the management and potentially the reversal of cardiorespiratory complications in infants and children with established BPD.

ARTICLE HISTORY

Received 7 April 2020
Revised 10 June 2020
Accepted 27 June 2020

KEYWORDS



Bronchopulmonary dysplasia; exosome; extracellular vesicles; mesenchymal stem cells; regenerative medicine; neonatal; lung injury

Introduction


Bronchopulmonary dysplasia (BPD), a multifactorial chronic lung disease, is one of the most common complications associated with prematurity. It is characterized by restricted lung growth, immature pulmonary vasculature, abnormal pulmonary function [1-3], and in moderate-to-severe cases, it is associated with secondary pulmonary hypertension (PH) [4-6]. Notable advancements in neonatal medicine have improved the survival and outcome of infants born at very low gestational age [7], but as a consequence have contributed to the increased occurrence of BPD [8]. Consequently, the modern day neonatal intensive care unit (NICU) witnesses the presentation of ever-more

immature lungs, further complicating the challenge of preventing, treating and reversing neonatal lung injury. To date, effective treatment strategies remain absent.

On this note, mesenchymal stromal cells (MSCs) have shown promise in numerous preclinical models of neonatal cardiorespiratory disease (reviewed in [3,9-13]). It is now recognized that MSCs afford their therapeutic effects through paracrine actions [14-16], specifically small extracellular vesicles (sEVs), a class of EVs which includes exosomes [17,18]. We [18] and others [19-21] have reported that early administration of purified human MSC-sEVs (MEx) improves core histological and functional outcomes in experimental BPD. Additional meritorious actions of MEx-based

CONTACT Stella Kourembanas  Stella.Kourembanas@childrens.harvard.edu  Division of Newborn Medicine, Boston Children's Hospital, Boston, MA 02115, USA

^{*}Senior authors contributing equally to this article.

 Supplemental material for this article can be accessed [here](#).

© 2020 The Author(s). Published by Informa UK Limited, trading as Taylor & Francis Group on behalf of The International Society for Extracellular Vesicles. This is an Open Access article distributed under the terms of the Creative Commons Attribution-NonCommercial License (<http://creativecommons.org/licenses/by-nc/4.0/>), which permits unrestricted non-commercial use, distribution, and reproduction in any medium, provided the original work is properly cited.

therapies have been demonstrated in several preclinical models where cardio-respiratory impairment and inflammation prevail [3,13,22–25].

To date, preclinical studies have focused on the preventative capacity of MEx, highlighting the beneficial effects of early MEx intervention. BPD is no longer considered a disease specific to the neonatal period but a complex multifactorial condition with lifelong cardio-respiratory consequences [13,26]. Thus, from a clinical perspective, in addition to preventing BPD, reversal of hyperoxia (HYRX)-induced lung injury is highly important. Here, using an established murine neonatal HYRX-induced lung injury model, we report that administration of MEx following a prolonged HYRX-insult improves core features of experimental BPD, restoring lung architecture and pulmonary blood vessel count, decreasing pulmonary fibrosis and vascular muscularization, ameliorating PH and improving exercise capacity.

Methods

Study approval

Animal experiments were approved by the Boston Children's Hospital Institutional Animal Care and Use Committee.

Tissue culture

Human umbilical cord Wharton's Jelly MSCs (WJMSCs) were isolated using a modified explant method, as described [27]. In brief, an umbilical cord was rinsed twice with Dulbecco's phosphate-buffered saline (dPBS, Invitrogen, MA, US), cut longitudinally and arteries and vein were removed. The soft gel tissues were finely dissected into small pieces (~3–6 mm²) and individually placed on 193 mm² tissue culture dishes (24-well plate) with α -Modified Eagle Medium (α MEM, Invitrogen, MA, US) supplemented with 20% foetal bovine serum (FBS, Invitrogen, MA, US), 2 mM L-glutamine and penicillin/streptomycin, and incubated for 12 days at 37°C in a humidified atmosphere of 5% CO₂. After periodic addition of supplemented α MEM, umbilical cord tissue was carefully removed. Plates were washed with media (x3); the plastic adherent cell colonies were trypsinized and maintained in culture in α MEM, supplemented with 10% foetal bovine serum, 2 mM L-glutamine and penicillin/streptomycin. At passage 4, WJMSCs were expanded to 10-stack Corning CellSTACK® cell culture chambers that occupied a cell growth area of 6360 cm² (Sigma, PA, US). Importantly, several umbilical cords were used;

each gave rise to individual MSC colonies. A different MEx preparation was used in each independent *in vivo* experiment.

Cell surface characterization and *in vitro* differentiation capacity

Cell surface characterization was carried out at passage 4 using flow cytometry. Antibodies used for cytometric analysis were obtained from BioLegend, CA, US and BD Biosciences, MA, US. Here, WJMSCs were selected for the expression of established MSC markers using labelled antibodies including APC/FITC-conjugated CD105, FITC-conjugated CD90, PE-conjugated CD44 and APC-conjugated CD73 and the absence of FITC-conjugated CD11b, PE-conjugated CD31, PE-conjugated CD34 and PE-conjugated CD45 using a set of fluorescently conjugated antibodies (Figure S1). Flow cytometry was performed using a BD™ LSR II flow cytometer, equipped with 407 nm, 488 nm and 640 nm lasers and BD FACS Diva software (v 5.0.3). The differentiation potential of WJMSC cultures to osteocyte and adipocyte lineages was assessed using StemPro®, osteogenesis and adipogenesis differentiation kits, respectively (ThermoFisher Scientific), as per manufacturer's instructions (Figure S1).

Extracellular vesicle (EV) nomenclature, harvest and isolation

Isolation and characterization of sEVs was in accordance with the 2018 Minimal Information for Studies of Extracellular Vesicles (MISEV) [28,29], as outlined by the International Society for Extracellular Vesicles (ISEV). Herein, MEx are defined by the following biophysical properties: sEVs that occupy a diameter of ~40–150 nm, have a density of ~1.18 g/ml and express established exosome markers such as ALIX, TSG101, CD81, CD9, CD63 and Flotillin-1 (FLOT-1).

MEx were isolated from MSC culture supernatants (conditioned media (CM)) after 36-h incubation in serum-free media as previously described [18,30]. Briefly, following differential centrifugation to eliminate cells (300 × g for 10 min), cellular debris (3,000 × g for 10 min) and related apoptotic detritus (13,000 × g for 30 min), CM were concentrated by filtration. Here, MSC-CM were concentrated 50-fold by tangential flow filtration (TFF) using a modified polyethersulfone (mPES) hollow fibre with 300 kDa MW cut-off (Spectrum Labs, Irving TX). EVs were further purified using OptiPrep™ (iodixanol) cushion density flotation. Specifically, an iodixanol gradient was prepared by floating 3 ml of 10% (w/v) iodixanol solution containing NaCl (150 mM) and

25 mM Tris:HCl (pH 7.4) over 3 ml of 55% (w/v) iodixanol solution. Concentrated CM (6 ml) were floated on top of the iodixanol cushion and ultra-centrifuged using a SW 40 Ti rotor for 3.5 h at $100,000 \times g$ at 4°C . Twelve fractions (1 ml each) were collected from the top of the gradient for immediate characterization or frozen ($-1^{\circ}\text{C}/\text{min}$) and kept at -80°C . The purified sEV population was enriched in fraction 9. Iodixanol fraction density was assessed by weight/volume ratio (g/ml).

Immuno-labelling and transmission electron microscopy (TEM)

To assess MEx morphology, an aliquot from the sEV preparation (5 μl) was adsorbed for 1 min to a carbon-coated grid (Electron Microscopy 170 Sciences, PA, US). Grids have been made hydrophilic by a 30-s exposure to a glow discharge. Excess liquid was removed with Whatman Grade 1 filter paper (Sigma), grids washed with one drop water, excess liquid removed as above and grids stained for 15 s with 1%

uranyl acetate. Adsorbed MEx were examined on a JEOL 1200EX transmission electron microscope (TEM), and images were recorded with an AMT 2 k CCD camera.

For immunogold labelling, MEx were absorbed for 5 min onto a glow-discharged carbon-coated grid and incubated in 1% bovine serum albumin (BSA (w/v)) for 10 min at room temperature. Next, MEx were incubated with human anti-CD63 or anti-CD81 (BD Pharmingen, MA, US) diluted 1:20 in 1% BSA (w/v) for 30 min at room temperature. Following $3 \times$ PBS washes, MEx preparations were incubated with rabbit anti-mouse IgG (AbCam) washed again $3 \times$ PBS and then incubated with Protein A-gold (10 nm, University Medical Centre Utrecht, Netherlands, 1:50 dilution) in 1% BSA (w/v) for 20 min at room temperature. After 2×5 min PBS washes and 3×5 water washes, excess liquid was removed with a filter paper and the samples stained with 1% uranyl acetate for 15 s prior to analysis using the JEOL 1200EX TEM, as described above.

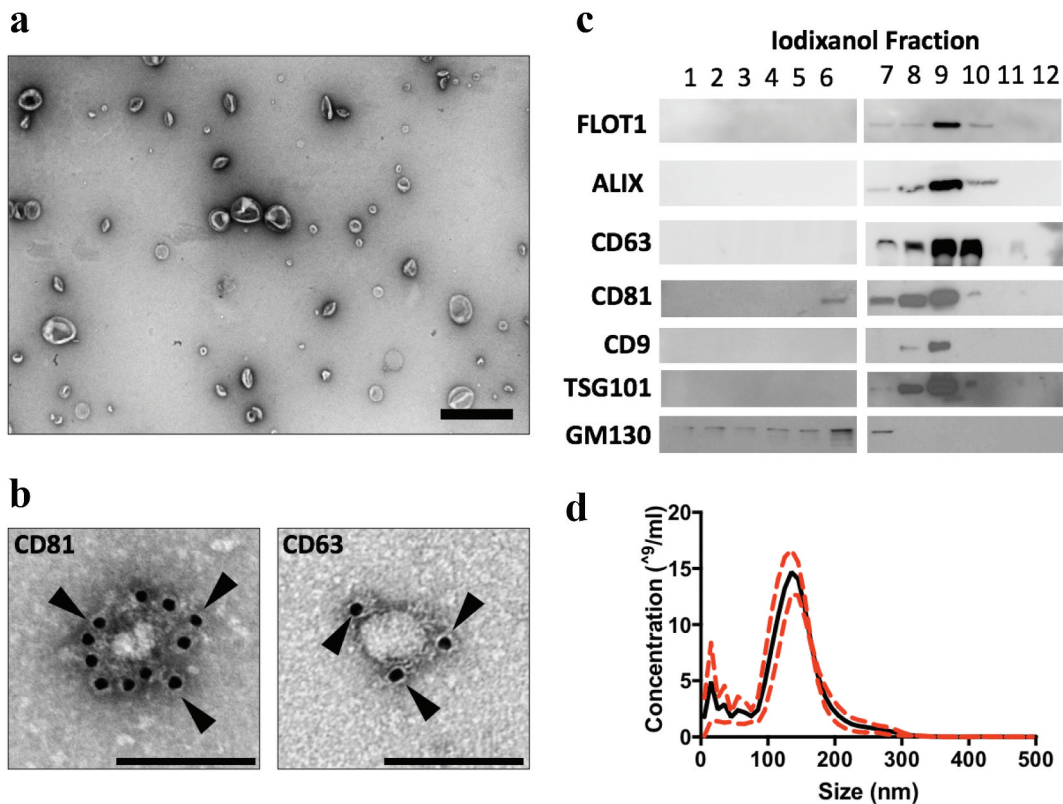


Figure 1. MEx purification and characterization. (a) Transmission electron microscopy (TEM) images demonstrating heterogeneous EV morphology (low magnification, $\times 15,000$, scale bar = 500 nm). (b) Gold-particle immunolabelled TEM images of anti-CD81 and anti-CD63 positive EVs (high magnification, $\times 30,000$, scale bar = 100 nm). Black arrows denote 10 nm gold conjugated with anti-CD81 or anti-CD63 antibody. (c) Representative images of immunoblotting analysis. Small EVs were purified in fraction 9, and expressed the established EV-associated markers, flotillin (FLOT-1), ALIX, TSG101 and tetraspanins (CD63, CD81 and CD9). MEx (fraction 9) immunoblots were negative for GM130. (d) Representative particle size and concentration distribution using nanoparticle tracking analysis (NTA). Red dotted line denotes SD.

Nanoparticle tracking analysis (NTA)

Size and concentration distributions of MEx were determined using nanoparticle tracking analysis (NTA, NanoSight LM10 system, Malvern instruments, MA, US), as previously described [13,31]. Samples were administered and recorded under controlled flow, using the NanoSight syringe pump and script control system, and for each sample, 5×30 s videos were recorded. Particle movement was analysed using NTA software (version 3.0). Camera shutter speed was fixed at 30.01 ms and camera gain to 500. Camera sensitivity and detection threshold were (11–14)– and (4–6)–, respectively. MEx samples were diluted in vesicle-free dPBS. Samples were run in triplicate, from which sEV distribution, size and mean concentration were calculated.

Immunoblotting

EV-associated proteins were separated on a 4–20% polyacrylamide gel (Bio-Rad, Hercules, CA) and then transferred onto 0.45 μ m PVDF membrane (Millipore, MA, US). All primary antibodies were purchased from Santa Cruz Biotech (CA, US) at dilutions recommended by the manufacturers.

Neonatal hyperoxia-induced lung injury model

Newborn mice (FVB strain) were exposed to hyperoxia (HYRX, 75% O₂) for 14 days (post-natal day (PN)14). Following HYRX exposure, mice returned to room air (NRMX). We compared mice that were exposed to HYRX, to animals that remained in NRMX for the study duration. A bolus intravenous (IV) MEx dose was administered at PN4 (classified as an early intervention), or alternatively, following prolonged HYRX-exposure, animals received serial MEx treatments over a 4-week period (PN18–39) on their return to NRMX (termed late intervention). Control groups included NRMX animals that received MEx and HYRX-exposed animals that received appropriate vehicle controls.

MEx dosing

Short-term outcome (PN28): Bolus “late” intervention

At PN18, MEx preparations (100 μ l) were injected (IV) via the tail vein. MEx preparations were diluted in dPBS to achieve a dose that corresponded to 1×10^6 cell equivalents. To assess the efficacy of a single “late” MEx intervention, mice were assessed

at PN28, as detailed above (schematic shown in Figure 2(a)).

Long-term outcome (PN60)

“Early” MEx intervention

At PN4, MEx preparations (50 μ l) were injected (IV) via the superficial temporal vein. MEx were diluted accordingly in dPBS to achieve a dose that corresponded to 0.5×10^6 cell equivalents. Mice which received a single “early” MEx intervention were assessed at PN60 (schematic shown in Figure 3(a)). Mice that received an “early” MEx treatment were compared to mice that received serial “late” treatments (as detailed below), and their respective controls.

Serial “late” MEx intervention

HYRX-exposed animals were administered four MEx treatments, after the HYRX-insult had occurred, over a 4-week period (PN18–39). MEx preparations (100 μ l) were injected (IV) via the tail vein (1×10^6 cell equivalents). Mice which received serial MEx doses after prolonged HYRX-exposure were assessed at PN60, as detailed above (schematic shown in Figure 3(b)). MEx dosing is further described in Table S1.

Notably, separate sets of experiments were performed to assess short-term and long-term outcomes. Our rationale for arriving at the selected MEx doses was based on previous findings [15,17,18,30], and is further detailed in the online supplement.

Hyperoxia (HYRX) chamber

Neonatal pups were pooled and exposed to 75% O₂ in a plexiglass chamber or to room air beginning at PN1 and continuing for 14 days (PN1–14). Ventilation was adjusted by an oxycycler controller (Biospherix, NY, US) to remove CO₂ so that it did not exceed 5000 ppm (0.5%). Ammonia was removed by ventilation and charcoal filtration through an air purifier. Dams were randomly rotated between room air (NRMX) and HYRX chambers every 48 h to prevent excessive O₂ toxicity to the adult mice. Litter sizes were evenly matched.

Lung tissue perfusion, dissection and histology

Following anaesthesia with 60 mg/kg pentobarbital (intraperitoneal (IP)), lungs were perfused with PBS through the right ventricle (RV) at a constant pressure of 25 cmH₂O. The left lung was carefully removed and stored at -80° C. The right lung was inflated to a fixed pressure of 15–20 cm H₂O with 4% paraformaldehyde

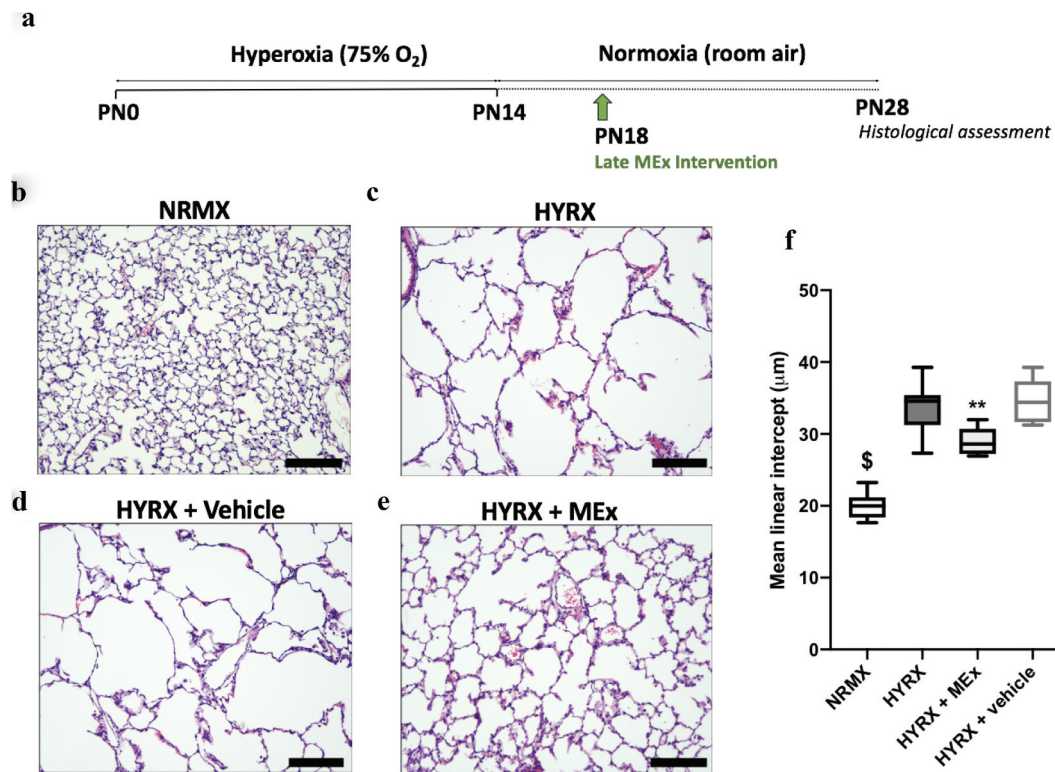


Figure 2. A bolus MEx treatment partially restores HYRX-induced alveolar simplification. Schematic of experimental model shown in (a). Briefly, newborn FVB mice were exposed to hyperoxia (HYRX) (75% O₂) for 14 days. HYRX-exposed mice were compared to mice that remained at NRMX (room air). MEx were delivered intravenously (IV) following the HYRX-insult at PN18. Short-term outcomes were assessed at PN28. Harvested lung sections were stained for haematoxylin and eosin (H&E) to assess lung architecture (b–e). Quantification of mean linear intercept (MLI, μm) represents a surrogate of average air space diameter (f). $n = 5–12$ per group, $**p < 0.01$, $^{\$}p < 0.0001$ vs. HYRX group. Scale bar = 100 μm.

(PFA) *in situ* and stored in 4% PFA overnight. Fixed lung tissue was transferred to 75% ethanol (EtOH) before subsequent processing and paraffin embedding for sectioning as four distinct right lung lobes (services provided by: Rodent Histopathology Core Facility – Harvard Medical School and ServiceBio (Woburn, MA)).

Lung parenchymal and vascular morphometry, immunofluorescence and immunohistochemistry

Following lung fixation with PFA (4% w/v), lung sections were analysed for histology. Lung sections were stained with Haematoxylin & Eosin (H&E) and Masson's Trichrome (collagen deposition). Randomly selected areas (10–20 fields) from 5 μm thick lung sections were captured at 100× (H&E) and 200× (Masson's Trichrome) magnification using a Nikon Eclipse 80i microscope (Nikon, Tokyo, Japan). Calibrations for the images were done by acquiring standard micrometre images using the same magnification. Large airways and vessels were avoided for the

lung morphometry. To measure mean linear intercept (MLI), a grid with parallel lines spaced at 58 μm was then overlaid onto the image, and the length of each chord, defined by the intercept with alveolar walls. The volume density (tissue density) of alveolar wall tissue was determined by a point-counting method using a computer-generated 30 × 30 grid superimposed to each image. The thickness of the alveolar septum was calculated by measuring the fibre breadth (area/length). The degree of collagen deposition was measured and expressed as percentage of collagen deposition per total septal area. All parameters were recorded using Metamorph software v.6.2 r (Universal Imaging, Downingtown, PA).

The loss of lung microvasculature was determined by counting the number of von Willebrand factor (vWF)-positive vessels (<350 μm) in 8–12 random images at 100× magnification using Metamorph software. Tissue sections were rehydrated and subjected to unmasking with 10 mM citrate buffer, and then incubated with primary antibody (Dako; polyclonal vWF Ab, 1:200). Afterwards, slides were washed and

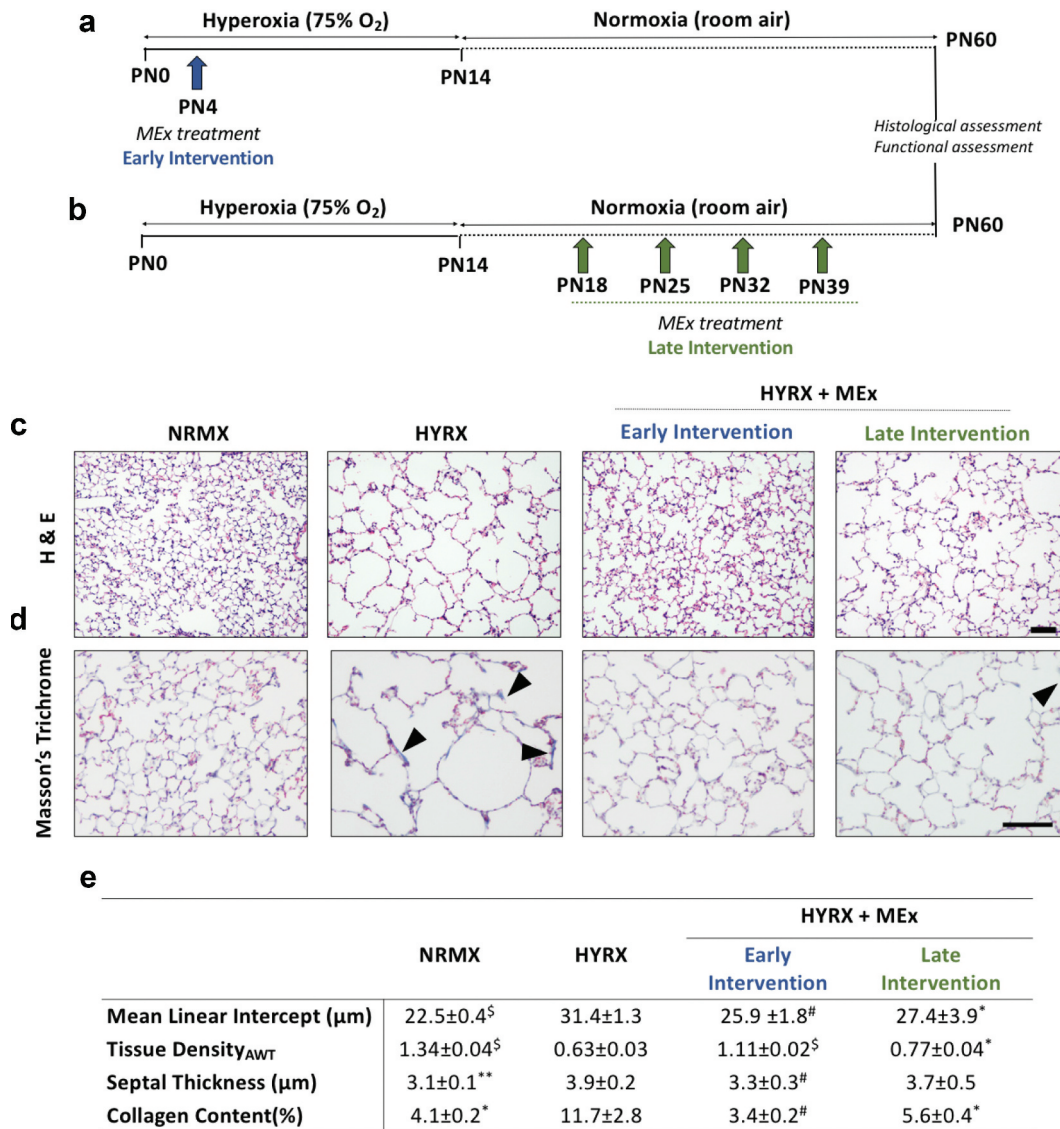


Figure 3. MEx treatment prevents and reverses alveolar abnormalities and ameliorates pulmonary fibrosis. Schematic of experimental model showing early MEx intervention (a) and late (reversal) MEx interventions (b). Long-term outcomes were assessed at PN60. Harvested lung sections were stained for (c) haematoxylin & eosin (H&E) to assess lung architecture and (d) Masson's trichrome to evaluate septal collagen deposition (arrows highlight collagen deposition). (e) Quantification of lung architecture was by assessment of mean linear intercept (MLI, μm), tissue density (AWT: alveolar wall thickness) and septal thickness (μm). Collagen deposition was used as a surrogate of pulmonary fibrosis and was reported as % of septal area. Arrows denote collagen deposition. $n = 6-12$ per group, * $p < 0.05$, ** $p < 0.01$, # $p < 0.001$, § $p < 0.0001$ vs. HYRX group. H&E scale bar = 100 μm. Masson's Trichrome scale bar = 50 μm.

incubated with cyanine-5 (Cy5)-conjugated donkey anti-rabbit (1:500) antibody.

To assess pulmonary vascularization, immunohistochemistry (IHC) analysis of alpha smooth muscle actin (α-SMA) was performed. Briefly, lung tissue sections were de-paraffinized in xylene and rehydrated. Tissue slides were treated with 0.3% H₂O₂ in methanol to inactivate endogenous peroxidases and blocked with horse serum for 20 min. After incubating with monoclonal anti-mouse α-SMA antibody (Sigma, MO, US) at

a dilution of 1:125, secondary antibodies and peroxidase staining were applied according to manufacturer's instructions (Vector Laboratories, CA, US). The vessel wall thickness was assessed by measuring α-SMA positive staining in blood vessels in ~15 sections captured at 400× magnification. The wall thickness was measured using Metamorph software and compared between groups using the following equation: Medial thickness index (MTI) = $100 \times (\text{area}_{[\text{ext}]} - \text{area}_{[\text{int}]}) / \text{area}_{[\text{ext}]}$. Area_[ext] and area_[int] denote the areas within the external

and internal boundaries of the α -SMA layer, respectively. For histological analysis, investigators were blinded to experimental groups. For blinded investigators, the intra- and inter-assay coefficients of variations were both <5%.

Right ventricular hypertrophy assessment (Fulton's Index)

To quantify the degree of right ventricular hypertrophy (RVH), we assessed Fulton's Index and RV-to-body weight (BW) ratio, as described [18]. Fulton's Index was measured as the ratio of RV weight over left ventricle (LV) plus septal (S) weight (RV/[LV+S]). Whole hearts were weighed first, before the RV wall was dissected and weighted, followed by the remaining LV and ventricular septum. RV:BW ratio was also used as an additional measure of RVH. Again, for physiological measurements, investigators were blinded to experimental groups.

Exercise capacity test

Exercise capacity tests were run to a predetermined protocol modified from van Haaften and colleagues [16]. Exercise capacity testing was conducted at Boston Children's Hospital Animal Behaviour and Physiology Core. Briefly, following habituation to the treadmill (4 lane IITC rodent treadmill, CA, US), mice were subjected to an incremental treadmill challenge, going from 3 m/min to 12 m/min over a 13-min period. We recorded the ability of mice to complete the challenge and/or the time to exhaustion. At the lower end of the treadmill apparatus was an electric shock pad which was applied as a negative reinforcer. Exhaustion was defined as the animals hitting and remaining on the shock pad for 4 consecutive seconds.

Statistics

Data were reported as Mean \pm SEM unless stated otherwise. Differences between different experimental groups were compared by ANOVA followed by Bonferroni's multiple comparison test using GraphPad Prism (v6.0; GraphPad, CA, US). Investigators were blinded to experimental groups for histological analysis and physiological measurements. Significance was considered at $p < 0.05$. For *in vivo* studies, we based our sample size calculations on previous work [15,18], suggesting that detection of a 15% improvement in lung architecture (assessed by mean linear intercept; MLI), with >90% power at the 5% α -level, requires a minimum of five animals per group.

Results

MEx nomenclature, purification and characterization

EVs were isolated from concentrated primary human WJMSC-CM using an iodixanol (IDX) density gradient. MEx occupied a density of ~ 1.16 – 1.18 g/ml. TEM and NTA of MEx preparations revealed a heterogeneous EV population that occupied a diameter of ~ 40 – 150 nm and conformed to the typical morphological features of sEVs (Figure 1(a,d)). Immunoblotting coupled with gold immunolabelling TEM confirmed that MEx expressed established EV-associated markers including ALIX, TSG101, tetraspanins (CD63, CD81, CD9) and flotillin-1 (FLOT-1) whilst being negative for GM130, a Golgi apparatus protein that is not present in MEx (Figure 1(b,c)). To aid interstudy comparison, MEx represents a heterogeneous sEV population derived from primary human WJMSCs, that conforms to the biophysical characteristics detailed above.

A bolus dose of MEx partially restores HYRX-induced alveolar simplification

Neonatal lung injury was inflicted by exposing newborn mice HYRX (75% O₂) for 14 days (PN1-14). Following exposure to HYRX, mice were returned to room air (NRMX) and harvested at PN28. As anticipated, 14 days of HYRX exposure resulted in a lung injury phenotype that resembles the clinical BPD presentation witnessed in the modern-day NICU. To assess alveolar simplification, a hallmark of BPD, we determined the MLI value across all experimental groups. HYRX-control mice presented with an elevated MLI value when compared to the NRMX-control group (33.66 ± 3.4 μm vs. 20.4 ± 1.8 μm , $p < 0.0001$, respectively, Figure 2(b,c)). To test the regenerative capacity of MEx, we first treated HYRX-exposed animals with a single IV dose of MEx at PN18. Compared to the HYRX-control group, a single dose of MEx administered after the HYRX exposure considerably improved alveolarization (28.97 ± 1.9 μm , $p < 0.01$, Figure 2(d)) whereas vehicle control had no ameliorative effect on lung architecture (34.48 ± 3.2 μm , $p > 0.05$, Figure 2(e)). In accordance with our previous data [18], MEx treatment had no impact on the lung architecture of NRMX-animals (data not shown).

Serial MEx interventions delivered after prolonged HYRX exposure dramatically improved alveolarization and pulmonary fibrosis

Considering the robust therapeutic impact of a single late MEx dose, we next challenged the ability of MEx to reverse the long-term destructive pulmonary effects of perinatal HYRX exposure by delivering consecutive MEx doses (termed “late” intervention) and assessing lung injury at PN60. In parallel, we compared the effectiveness of our serial late MEx administrations to a single early MEx treatment delivered at PN4 (schematic shown in [Figure 3\(a,b\)](#)).

To provide a comprehensive assessment of both MEx interventions, we assessed MLI, tissue density (alveolar wall thickness), septal thickness and septal collagen disposition at PN60 (long-term endpoint). As predicted, alveolar simplification persisted in HYRX-exposed mice ([Figure 3\(c\)](#)). Compared to NRMX-controls, the HYRX-control group presented with a persistent destructive lung architecture characterized by an elevated MLI and septal thickness and reduced tissue density ($p < 0.01$, [Figure 3\(c,e\)](#)). HYRX-exposed mice that received the early MEx intervention presented with an “almost” completely restored lung architecture. This was confirmed by quantification of MLI, septal thickness and tissue density ([Figure 3\(c,e\)](#) $p < 0.001$). Mice that were treated with serial MEx doses which were delivered after the HYRX-induced injury presented with a substantially improved lung parenchyma. Albeit to a lesser degree than the early intervention, compared to the HYRX-control group, animals that received the late MEx intervention exhibited superior MLI and septal thickness measurements ($p < 0.05$). Tissue density changes did not reach significance ([Figure 3\(e\)](#), $p > 0.05$).

Lung sections were also stained with Masson’s Trichrome to assess the anti-fibrotic actions of MEx. HYRX-exposed mice presented with an elevated amount of septal collagen deposition compared to NRMX-animals (11.7 ± 2.8 vs. $4.1 \pm 0.2\%$; $p < 0.05$, respectively, [Figure 3\(d,e\)](#)). The HYRX-induced elevation in collagen deposition was blunted by the early MEx treatment ($3.4 \pm 0.2\%$, $p < 0.001$), and was also improved with the late MEx ($5.6 \pm 0.4\%$, $p < 0.05$, [Figure 3\(d,e\)](#)).

MEx therapy reverses HYRX-induced elevations in pulmonary vascular muscularization and rescues peripheral pulmonary microvascular loss

In moderate to severe cases of BPD, secondary PH prevails and is associated with increased mortality [4,5].

Thus, we chose to assess vascular and physiological parameters to determine the impact of our MEx interventions on PH. Firstly, to determine peripheral pulmonary vessel number, we undertook vWF staining in the lung sections at PN60. Compared with NRMX-mice, HYRX-exposed animals presented with a significantly reduced number of peripheral blood vessels ($<350 \mu\text{m}$ diameter) (11.7 ± 3.9 vs. 3.9 ± 0.45 blood vessels/field, respectively, $p < 0.0001$). The early MEx intervention improved blood vessel count to level akin to their NRMX counterparts (7.5 ± 0.9 blood vessels/field, $p < 0.05$). Interestingly, the late MEx intervention had a similar efficacy to the early MEx treatment, partially rescuing the HYRX-induced loss of blood vessels (7.2 ± 0.9 blood vessels/field, respectively, $p < 0.05$, [Figure 4\(a,b\)](#)).

To assess the effect of HYRX-exposure on pulmonary vascular remodelling, we undertook α -SMA staining in lung sections of mice at PN60. As predicted, compared to NRMX-mice, HYRX-exposure induced pronounced vascular muscularization (22.58 ± 3 MTI vs. 51.13 ± 6 MTI, $p < 0.0001$, respectively). Impressively, the HYRX-exposed animals that received either the late or early MEx intervention presented with MTI values akin to the NRMX counterparts (33.90 ± 5 MTI and 25.37 ± 4 MTI, $p < 0.0001$, respectively, [Figure 4\(c,d\)](#)).

Early and late MEx interventions blunt right ventricular hypertrophy

To investigate the presence of HYRX-induced PH, we assessed Fulton’s index (RV/LV+S), a measure of RVH. Here, compared to the NRMX-control group, HYRX-control animals presented with an elevated Fulton’s Index (0.23 ± 0.02 vs. 0.32 ± 0.03 , $p < 0.0001$, respectively). Interestingly, both the early and the late MEx interventions dramatically improved the HYRX alterations in RVH to the same degree (early intervention: 0.25 ± 0.03 ; late intervention: 0.25 ± 0.03 , $p < 0.001$, [Figure 5\(a\)](#)). A similar trend was recapitulated when assessing RV:BW, although this trend did not achieve significance ($p > 0.05$, [Figure 5\(b\)](#)). Across all experimental groups, the severity of peripheral pulmonary blood vessel loss and burden of vascular remodelling was associated with Fulton’s index ($p = 0.0001$, $r = 0.437$ and $p = 0.02$, $r = 0.525$, respectively).

MEx administration improves functional exercise capacity

In order to determine the functional impact of such robust histological and physiological changes, we next undertook exercise capacity testing in our experimental groups at PN60, a surrogate for cardio-pulmonary

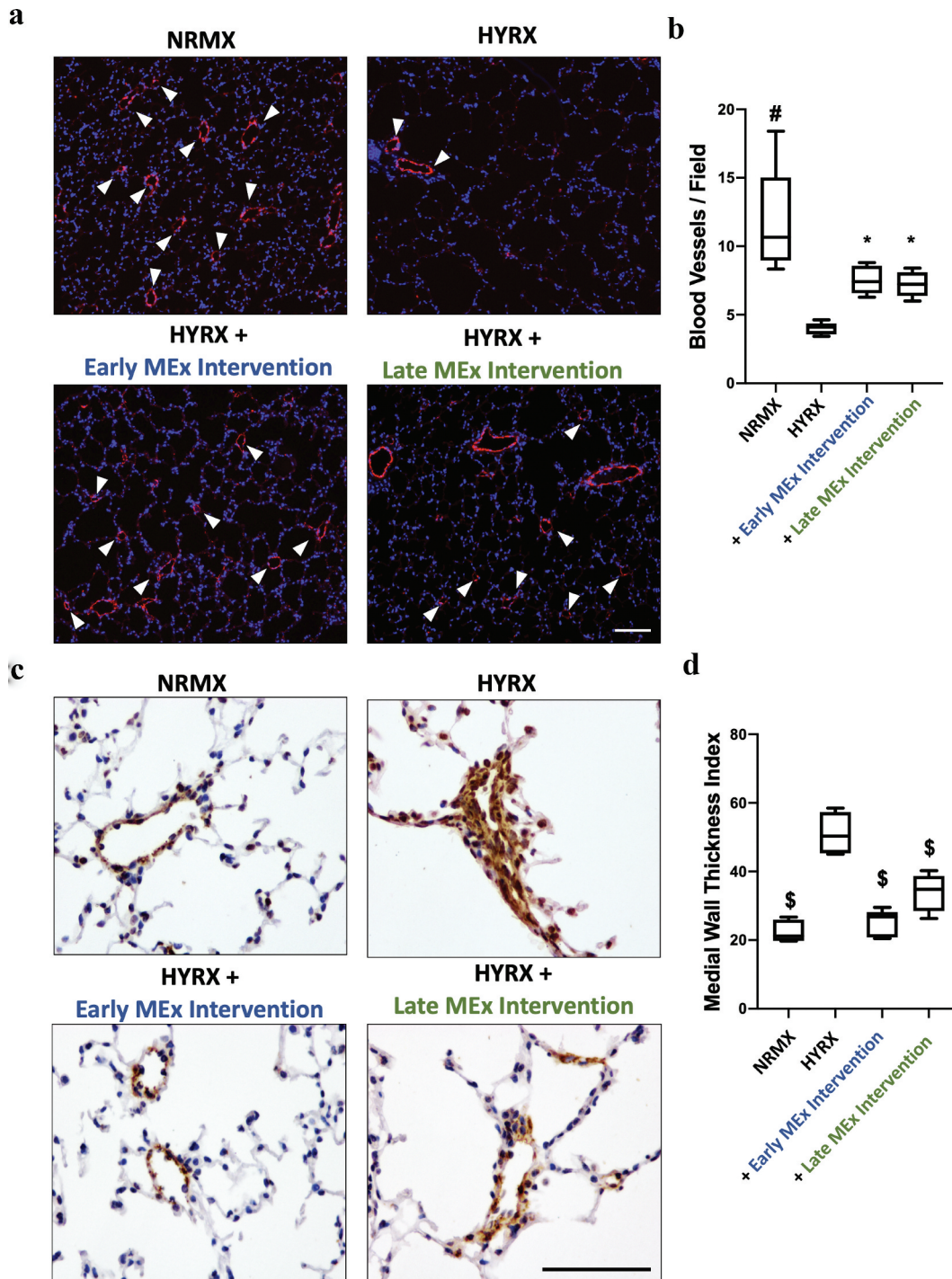


Figure 4. Early and late MEx administration improves peripheral pulmonary blood vessel count and pulmonary vascular muscularization. Long-term outcomes were assessed at PN60. Harvested lung sections were stained von Willebrand factor (vWF) (a) or α -smooth muscle actin (α -SMA) (c) to assess the effect of HYRX on peripheral pulmonary blood vessel loss and pulmonary vascular remodelling, respectively. Arrows highlight vWF-stained pulmonary vessels. (b) For quantification of blood vessels, values are expressed as the average blood vessel count per field. (d) Medial thickness index (MTI) = $100 \times (\text{area}_{[\text{ext}]} - \text{area}_{[\text{int}]}) / \text{area}_{[\text{ext}]}$. $\text{Area}_{[\text{ext}]}$ and $\text{area}_{[\text{int}]}$ denote the areas within the external and internal boundaries of the α -SMA layer, respectively. vWF scale bar = 100 μm . α -SMA scale bar = 75 μm . $n = 6\text{--}12$ per group. * $p < 0.05$, # $p < 0.001$, § $p < 0.0001$ vs. HYRX group.

function. Using a predetermined protocol, we recorded the ability of mice to complete the exercise challenge and/or the distance achieved until exhaustion, as

outlined in the methods. Compared to NRMX-animals, the HYRX-exposed mice presented with a diminished exercise capacity ($p < 0.0001$), which

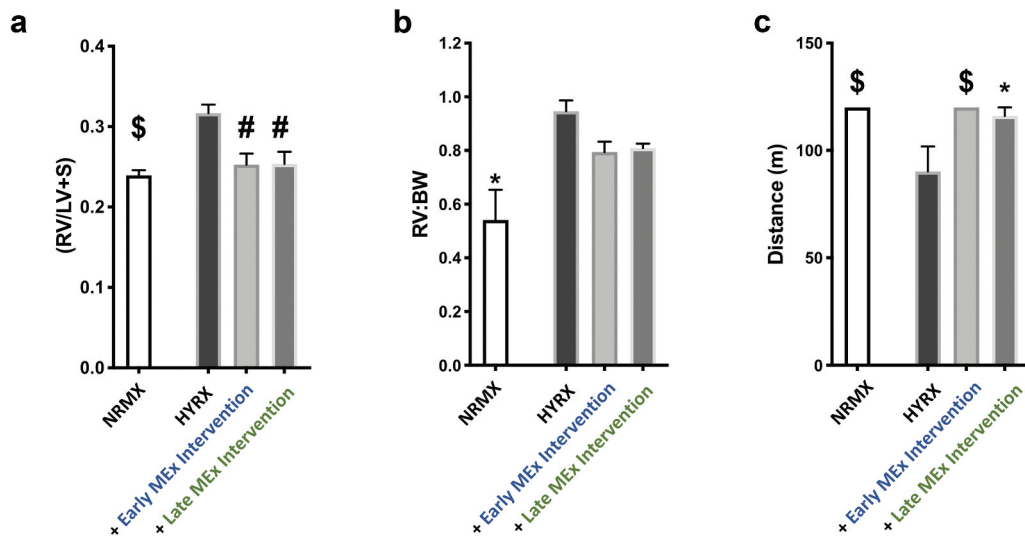


Figure 5. MEx treatment ameliorates right ventricular hypertrophy (RVH) and improves functional exercise capacity. (a) Fulton's Index measurements (ratio of right ventricle (RV) weight over left ventricle (LV) plus septum weight) and right ventricle-to-body weight ratio (RV:BW) (b) were undertaken to assess the degree of right ventricular hypertrophy (RVH), an index of pulmonary hypertension (PH). (c) Exercise capacity testing was carried out across all experimental groups to investigate the functional benefits of MEx. Mean \pm SEM, $n = 4$ –12 per group, * $p < 0.05$, # $p < 0.001$, \$ $p < 0.0001$ vs. HYRX group.

was restored by the early MEx intervention ($p < 0.0001$) and was also ameliorated by the late MEx intervention ($p < 0.05$, Figure 5(c)).

Discussion

BPD is a multifactorial disorder that occurs almost exclusively in preterm infants that required oxygen therapy and mechanical ventilation in the perinatal period. Although the disorder lacks a known aetiology, probable prenatal origins include preeclampsia, oligohydramnios and chorioamnionitis [32–37]. HYRX-induced lung injury often occurs in the newborn when endotracheal intubation, oxygen supplementation, mechanical ventilation and subsequently oxidative stress cannot be avoided due to respiratory failure. Notwithstanding the obvious benefits of preventative treatments, the ability of MEx to reverse the major pathological hallmarks of established BPD is highly attractive for current clinical practices.

In this study, we demonstrate that administration of “purified” MEx following prolonged HYRX-exposure radically improved lung architecture, decreased pulmonary fibrosis, restored peripheral pulmonary blood vessel loss and ameliorated pulmonary vascular muscularization. Moreover, we are the first to demonstrate that a “late” MEx intervention improves the BPD architectural injury and also provides favourable functional outcomes, ameliorating associated RVH and improving exercise capacity. Of interest, an isolated case study

involving a 10-month-old female BPD patient with superimposed acute respiratory distress syndrome found that a single dose of MSCs was associated with dramatic reduction in lung fibrosis assessed by computed tomographic scan imaging of the chest and pronounced clinical improvement of lung function [38]. Our findings are also in agreement with previous studies that have shown beneficial effects following “early” MEx interventions in experimental BPD [18–21], and recent preclinical data that demonstrated treatment of the adult rat BPD lung with MSCs improved lung injury when administered in multiple doses or at an early stage of adulthood [39]. In accordance, previous studies have demonstrated that the MSC secretome (MSC-CM) is able to partially revert core features of neonatal murine BPD [15,16]. This study supports and extends such observations to show that the main therapeutic vector in the MSC-CM is represented by sEVs.

Mice are born in the saccular stage of lung development (between embryonic day (E)17.5 and PN5), reflecting the pulmonary developmental stage of a human preterm neonate of ~24–28 weeks gestation (reviewed in [40]). Of note, the “early” MEx intervention was administered at PN4. In contrast, the late MEx intervention was delivered between PN18–39, translating to a more mature human lung development stage, ranging from a juvenile-adolescent to a mature adult lung [40]. When compared side-by-side, mice that received early MEx treatment presented with a more profound improvement in the degree of alveolarization and

fibrosis, compared to mice that received serial MEx doses following the HYRX-insult. Thus, this body of work supports a growing consensus that an early intervention is critical for optimal efficiency in preserving lung development [18,41]. Of note, it remains unclear if serial “early” MEx interventions provide any added benefit and should be investigated in future studies. Similarly, Álvarez-Fuente and colleagues reported on the off-label use of repeated IV MSC doses in two infants with advanced and severe BPD, concluding that the administration of repeated MSC doses was feasible, non-toxic and maybe associated with a decrease in the levels of pro-inflammatory cytokines in peripheral blood cells [42]. Interestingly, in our study, we found that the “late” MEx intervention was just as effective at restoring pulmonary blood vessel number and ameliorating RVH as the “early” MEx treatment.

BPD is no longer considered a disorder of the neonatal period, but a complex condition that is associated with life-long cardio-respiratory morbidity [43]. Upon assessment of long-term pulmonary complications (PN60), our study demonstrated that both early and late MEx interventions improved long-term cardio-respiratory function, reversing RVH and improving exercise capacity. Accordingly, previous preclinical reports have shown that early MEx interventions improve lung function [18]. BPD patients present with pulmonary abnormalities that persist throughout childhood, and even into adulthood [43,44]. As such, there is a growing awareness that infants and young adults who were former BPD patients appear prone to develop asthma and chronic obstructive pulmonary disease (COPD) [43–46]. Taken together, our studies may support the rationale for MEx-based therapies in disorders where parenchymal injury has already occurred. In line with this, emerging evidence suggests that MEx provide beneficial histological effects in models of emphysema [47] and can reverse core features of experimental pulmonary fibrosis [30] and PH [48]. However, it remains unclear if a “very late” MEx intervention would provide any benefit in experimental BPD and should be addressed in future studies.

Detailed mechanisms by which MEx afford their beneficial effects remain incompletely understood. Moreover, it is not clear whether the “early” and “late” interventions share a common therapeutic mechanism of action. In experimental BPD, we and others have noted that pulmonary macrophages (Mφs) occupy an “M2-like” phenotype, that can persist for several months following HYRX-exposure [18,30,49]. Considering the potent immunomodulatory actions of MEx [50–52], future studies should consider if modulating

a persistently dysregulated monocyte/Mφ phenotype can inhibit any further fibrosis and reprogramme the lung milieu to afford reparative actions. Furthermore, considering their diverse functions across multiple experimental models, the pursuit for a single active ingredient is arguably futile. Rather, MEx likely contain an orchestra of bioactive components that synergistically provide the therapeutic actions, and that this is likely in a target cell and model/disease-specific manner. Our ongoing studies are aimed at deciphering the therapeutic mechanism-of-action of MEx.

Although encouraged by such findings, we acknowledge several limitations of this work. Firstly, we only administered MEx IV. Other studies have shown that early MEx interventions delivered by intraperitoneal or intratracheal administration routes provide similar therapeutic benefits as IV dosing [19–21]. Future studies should consider employing different preclinical BPD models and/or choosing different routes of administration that are more amenable to testing the efficacy of serial “early” MEx doses. Future studies should investigate how different administration routes impact MEx biodistribution and efficacy in parallel. Furthermore, we acknowledge that the beneficial actions of MSCs may not be limited to such paracrine mechanisms. Indeed, in other experimental models, the beneficial actions of MSCs have been attributed to either different EV subsets such as larger mitochondrial containing EVs, or through direct cell-to-cell contact [22,53,54]. Thus, considering every preclinical model of BPD is subject to its own advantages and limitations, we encourage the findings of this study to be judged in the context of the experimental model used.

In summary, we demonstrate that MEx prevent and reverse core features of experimental BPD, restoring lung architecture, decreasing fibrosis and pulmonary vascular muscularization, ameliorating PH and improving exercise capacity. Although future studies are needed to decipher mechanism of action, we demonstrate that delivery of MEx may not only be effective in the immediate neonatal period to promote normal lung development but may provide beneficial effects in infants and children with established BPD injury.

Author’s contributions

G.R.W. participated in study design and execution, data collection, analysis and manuscript writing; A.F.-G., M. R. and V.Y. participated in study execution, data collection and data analysis; X.L., M.E., and N.A. provided technical assistance; S.A.M. and S.K. contributed to study design, supervision of study execution, manuscript writing, and final article editing and approval.

Acknowledgments

The authors thank Ms. Janhavi Nadkarni (Boston Children's Hospital, Boston, MA) for providing technical assistance and blinded analysis.

Disclosure statement

No conflict of interest. SK and SAM are named inventors on intellectual property licensed by Boston Children's Hospital to United Therapeutics Corp.

Funding

Supported in part by National Institutes of Health grants R01HL146128, R01 HL055454 (S.K) and K99HL146986-01A1 (G.R.W), Charles H. Hood Foundation Major Grants Initiative to Advance Child Health (S.K), and a United Therapeutics Corp. Sponsored Research grant (S.K and S. A.M.), American Thoracic Society Unrestricted Foundation Grant (G.R.W) and The Little Giraffe Foundation Research Grant (G.R.W). Boston Children's Hospital Animal Behaviour and Physiology Core receives support from the Children's Hospital Intellectual and Developmental Disabilities Research Center (IDDRC); (CHB IDDRC 1U54HD090255).

References

- [1] Stenmark KR, Abman SH. Lung vascular development: implications for the pathogenesis of bronchopulmonary dysplasia. *Annu Rev Physiol.* 2005;67:623–661. Epub 2005/ 02/16.
- [2] Jobe AH, Bancalari E. Bronchopulmonary dysplasia. *Am J Respir Crit Care Med.* 2001;163(7):1723–1729. Epub 2001/ 06/13.
- [3] Mitsialis SA, Kourembanas S. Stem cell-based therapies for the newborn lung and brain: possibilities and challenges. *Semin Perinatol.* 2016;40(3):138–151. Epub 2016/ 01/19.
- [4] Khemani E, McElhinney DB, Rhein L, et al. Pulmonary artery hypertension in formerly premature infants with bronchopulmonary dysplasia: clinical features and outcomes in the surfactant era. *Pediatrics.* 2007;120(6):1260–1269. Epub 2007/ 12/07.
- [5] Del Cerro MJ, Sabate Rotes A, Carton A, et al. Pulmonary hypertension in bronchopulmonary dysplasia: clinical findings, cardiovascular anomalies and outcomes. *Pediatr Pulmonol.* 2014;49(1):49–59. Epub 2013/ 06/22.
- [6] Abman SH, Hansmann G, Archer SL, et al. Pediatric pulmonary hypertension: guidelines from the American Heart Association and American Thoracic Society. *Circulation.* 2015;132(21):2037–2099. Epub 2015/ 11/05.
- [7] Jain D, Bancalari E. Bronchopulmonary dysplasia: clinical perspective. *Birth Defects Res Part A, Clin Mol Teratol.* 2014;100(3):134–144. Epub 2014/ 03/01.
- [8] Stoll BJ, Hansen NI, Bell EF, et al. Trends in care practices, morbidity, and mortality of extremely preterm neonates, 1993–2012. *Jama.* 2015;314(10):1039–1051. Epub 2015/ 09/09.
- [9] Matthay MA, Anversa P, Bhattacharya J, et al. Cell therapy for lung diseases. Report from an NIH–NHLBI workshop, November 13–14, 2012. *Am J Respir Crit Care Med.* 2013;370–375. DOI:10.1164/rccm.201303-0522WS
- [10] Fung ME, Thébaud B. Stem cell-based therapy for neonatal lung disease: it is in the juice. *Pediatr Res.* 2014;75(1–1):2–7. Epub 2014/ 10/14.
- [11] Alvarez-Fuente M, Moreno L, Mitchell JA, et al. Preventing bronchopulmonary dysplasia: new tools for an old challenge. *Pediatr Res.* 2019;85(4):432–441. Epub 2018/ 11/23.
- [12] Kang M, Thebaud B. Stem cell biology and regenerative medicine for neonatal lung diseases. *Pediatr Res.* 2018;83(1–2):291–297. Epub 2017/ 09/19.
- [13] Willis GR, Mitsialis SA, Kourembanas S. “Good things come in small packages”: application of exosome-based therapeutics in neonatal lung injury. *Pediatr Res.* 2018;83(1–2):298–307. doi:10.1038/pr.2017.256. Epub 2017/ 10/07.
- [14] Aslam M, Baveja R, Liang OD, et al. Bone marrow stromal cells attenuate lung injury in a murine model of neonatal chronic lung disease. *Am J Respir Crit Care Med.* 2009;180(11):1122–1130. Epub 2009/ 08/29.
- [15] Hansmann G, Fernandez-Gonzalez A, Aslam M, et al. Mesenchymal stem cell-mediated reversal of bronchopulmonary dysplasia and associated pulmonary hypertension. *Pulm Circ.* 2012;2(2):170–181. Epub 2012/ 07/28.
- [16] van Haaften T, Byrne R, Bonnet S, et al. Airway delivery of mesenchymal stem cells prevents arrested alveolar growth in neonatal lung injury in rats. *Am J Respir Crit Care Med.* 2009;180(11):1131–1142. Epub 2009/ 08/29.
- [17] Lee C, Mitsialis SA, Aslam M, et al. Exosomes mediate the cytoprotective action of mesenchymal stromal cells on hypoxia-induced pulmonary hypertension. *Circulation.* 2012;126(22):2601–2611. Epub 2012/ 11/02.
- [18] Willis GR, Fernandez-Gonzalez A, Anastas J, et al. Mesenchymal stromal cell exosomes ameliorate experimental bronchopulmonary dysplasia and restore lung function through macrophage immunomodulation. *Am J Respir Crit Care Med.* 2018;197(1):104–116. Epub 2017/ 08/31.
- [19] Braun RK, Chetty C, Balasubramaniam V, et al. Intraperitoneal injection of MSC-derived exosomes prevent experimental bronchopulmonary dysplasia. *Biochem Biophys Res Commun.* 2018;503(4):2653–2658. Epub 2018/ 08/11.
- [20] Chaubey S, Thueson S, Ponnalagu D, et al. Early gestational mesenchymal stem cell secretome attenuates experimental bronchopulmonary dysplasia in part via exosome-associated factor TSG-6. *Stem Cell Res Ther.* 2018;9(1):173.
- [21] Porzionato A, Zaramella P, Dedja A, et al. Intratracheal administration of clinical-grade mesenchymal stem cell-derived extracellular vesicles reduces lung injury in a rat model of bronchopulmonary dysplasia. *Am J Physiol Lung Cell Mol Physiol.* 2019;316(1):L6–L19. Epub 2018/ 10/05.
- [22] Morrison TJ, Jackson MV, Cunningham EK, et al. Mesenchymal stromal cells modulate macrophages in

- clinically relevant lung injury models by extracellular vesicle mitochondrial transfer. *Am J Respir Crit Care Med.* **2017**;196(10):1275–1286. Epub 2017/ 06/10.
- [23] Fujita Y, Kadota T, Araya J, et al. Clinical application of mesenchymal stem cell-derived extracellular vesicle-based therapeutics for inflammatory lung diseases. *J Clin Med.* **2018**;7(10). Epub 2018/ 10/17. DOI:10.3390/jcm7100355.
- [24] Suzuki E, Fujita D, Takahashi M, et al. Therapeutic effects of mesenchymal stem cell-derived exosomes in cardiovascular disease. *Adv Exp Med Biol.* **2017**;998:179–185. Epub 2017/ 09/25.
- [25] Long Q, Upadhy D, Hattiangady B, et al. Intranasal MSC-derived A1-exosomes ease inflammation and prevent abnormal neurogenesis and memory dysfunction after status epilepticus. *Proc Nat Acad Sci.* **2017**;114(17):E3536–E45.
- [26] Thebaud B, Kourembanas S. Can we cure bronchopulmonary dysplasia? *J Pediatr.* **2017**;191:12–14. Epub 2017/ 09/26.
- [27] Seshareddy K, Troyer D, Weiss ML. Method to isolate mesenchymal-like cells from Wharton's Jelly of umbilical cord. *Methods Cell Biol.* **2008**;86:101–119. Epub 2008/ 04/30.
- [28] They C, Witwer KW, Aikawa E, et al. Minimal information for studies of extracellular vesicles 2018 (MISEV2018): a position statement of the International Society for Extracellular Vesicles and update of the MISEV2014 guidelines. *J Extracell Vesicles.* **2018**;7(1):1535750. Epub 2019/ 01/15.
- [29] Witwer KW, Van Balkom BWM, Bruno S, et al. Defining mesenchymal stromal cell (MSC)-derived small extracellular vesicles for therapeutic applications. *J Extracell Vesicles.* **2019**;8(1):1609206. Epub 2019/ 05/ 10.
- [30] Mansouri N, Willis GR, Fernandez-Gonzalez A, et al. Mesenchymal stromal cell exosomes prevent and revert experimental pulmonary fibrosis through modulation of monocyte phenotypes. *JCI Insight.* Epub 2019/ 10/04. **2019**;4(21). DOI:10.1172/jci.insight.128060
- [31] Willis GR, Connolly K, Ladell K, et al. Young women with polycystic ovary syndrome have raised levels of circulating annexin V-positive platelet microparticles. *Hum Reprod.* **2014**;29(12):2756–2763. Epub 2014/ 10/ 23.
- [32] Kim DH, Kim HS, Choi CW, et al. Risk factors for pulmonary artery hypertension in preterm infants with moderate or severe bronchopulmonary dysplasia. *Neonatology.* **2012**;101(1):40–46. Epub 2011/ 07/28.
- [33] Saugstad OD. Resuscitation of newborn infants: from oxygen to room air. *Lancet.* **2010**;376(9757):1970–1971. Epub 2010/ 07/29.
- [34] Hansen AR, Barnes CM, Folkman J, et al. Maternal preeclampsia predicts the development of bronchopulmonary dysplasia. *J Pediatr.* **2010**;156(4):532–536. Epub 2009/ 12/17.
- [35] Tang JR, Karumanchi SA, Seedorf G, et al. Excess soluble vascular endothelial growth factor receptor-1 in amniotic fluid impairs lung growth in rats: linking preeclampsia with bronchopulmonary dysplasia. *Am J Physiol Lung Cell Mol Physiol.* **2012**;302(1):L36–46. Epub 2011/ 10/18.
- [36] Watterberg KL, Demers LM, Scott SM, et al. Chorioamnionitis and early lung inflammation in infants in whom bronchopulmonary dysplasia develops. *Pediatrics.* **1996**;97(2):210–215. Epub 1996/ 02/01
- [37] Hansmann G. Neonatal resuscitation on air: it is time to turn down the oxygen tanks [corrected]. *Lancet.* **2004**;364(9442):1293–1294. Epub 2004/ 10/12.
- [38] Lin H-C, Wang -C-C, Chou H-W, et al. Airway delivery of bone marrow-derived mesenchymal stem cells reverses bronchopulmonary dysplasia superimposed with acute respiratory distress syndrome in an infant. *Cell Med.* **2018**;10:2155179018759434.
- [39] O'Reilly M, Mobius MA, Vadivel A, et al. Late rescue therapy with cord-derived mesenchymal stromal cells for established lung injury in experimental bronchopulmonary dysplasia. *Stem Cells Dev.* **2020**;29(6):364–371.
- [40] Nardiello C, Mizikova I, Morty RE. Looking ahead: where to next for animal models of bronchopulmonary dysplasia? *Cell Tissue Res.* **2017**;367(3):457–468. Epub 2016/ 12/06.
- [41] Willis GR, Kourembanas S, Mitsialis SA. Toward exosome-based therapeutics: isolation, heterogeneity, and fit-for-purpose potency. *Front Cardiovasc Med.* **2017**;4:63. Epub 2017/ 10/25.
- [42] Álvarez-Fuente M, Arruza L, Lopez-Ortego P, et al. Off-label mesenchymal stromal cell treatment in two infants with severe bronchopulmonary dysplasia: clinical course and biomarkers profile. *Cytotherapy.* **2018**;20 (11):1337–1344.
- [43] Stocks J, Hislop A, Sonnappa S. Early lung development: lifelong effect on respiratory health and disease. *Lancet Respir Med.* **2013**;1(9):728–742. Epub 2014/ 01/17.
- [44] Perez Tarazona S, Solano Galan P, Bartoll Alguacil E, et al. Bronchopulmonary dysplasia as a risk factor for asthma in school children and adolescents: a systematic review. *Allergol Immunopathol (Madr).* **2018**;46 (1):87–98. Epub 2017/ 07/03.
- [45] Schmalisch G, Wilitzki S, Roehr CC, et al. Development of lung function in very low birth weight infants with or without bronchopulmonary dysplasia: longitudinal assessment during the first 15 months of corrected age. *BMC Pediatr.* **2012**;12:37. Epub 2012/ 03/27.
- [46] Postma DS, Bush A, van den Berge M. Risk factors and early origins of chronic obstructive pulmonary disease. *Lancet.* **2015**;385(9971):899–909. Epub 2014/ 08/16.
- [47] Kim Y-S, Kim J-Y, Cho R, et al. Adipose stem cell-derived nanovesicles inhibit emphysema primarily via an FGF2-dependent pathway. *Exp Mol Med.* **2017**;49 (1):e284–e.
- [48] Klinger JR, Pereira M, Del Tatto M, et al. Mesenchymal stem cell extracellular vesicles reverse sugen/hypoxia pulmonary hypertension in rats. *Am J Respir Cell Mol Biol.* **2020**;62(5):577–587. doi:10.1165/rcmb.2019-0154OC. Epub 2019/ 11/14.
- [49] Yoder HE, Braun RK, Sobotik A, et al. Increased activation of M2 macrophages in 1 year-old rat lungs following neonatal hyperoxia exposure. *Faseb J.* **2017**;31 (1):872.3–3.
- [50] Chen W, Huang Y, Han J, et al. Immunomodulatory effects of mesenchymal stromal cells-derived exosome. *Immunol Res.* **2016**;64(4):831–840. Epub 2016/ 04/27.

- [51] Willis GR, Fernandez-Gonzalez A, Reis M, et al. Macrophage immunomodulation: the gatekeeper for mesenchymal stem cell derived-exosomes in pulmonary arterial hypertension? *Int J Mol Sci.* 2018;19(9). Epub 2018/ 08/29. DOI:[10.3390/ijms19092534](https://doi.org/10.3390/ijms19092534).
- [52] Kordelas L, Schwich E, Dittrich R, et al. Individual immune-modulatory capabilities of MSC-derived extracellular vesicle (EV) preparations and recipient-dependent responsiveness. *Int J Mol Sci.* 2019;20(7):1642.
- [53] Phinney DG, Di Giuseppe M, Njah J, et al. Mesenchymal stem cells use extracellular vesicles to outsource mitophagy and shuttle microRNAs. *Nature Commun.* 2015;6:8472.
- [54] Jackson MV, Morrison TJ, Doherty DF, et al. Mitochondrial transfer via tunneling nanotubes is an important mechanism by which mesenchymal stem cells enhance macrophage phagocytosis in the in vitro and in vivo models of ARDS. *Stem Cells.* 2016;34(8):2210–2223.